

# Fourth generation cryogenic neutral cluster beam apparatus for studying fundamental properties of metallic clusters

Lin Miao<sup>1#</sup>, Zhaojun Liu<sup>1#</sup>, Zeyang Chen<sup>1</sup>, Xiaohan Wang<sup>1</sup>, Ziwen Zhou<sup>1</sup>, Jinbo Zhao<sup>1</sup>, Shaozheng Fang<sup>1</sup>, Guangjia Yin<sup>1</sup>, Zezhao Jia<sup>1</sup>, Jin Liu<sup>1</sup>, Ramiro Moro<sup>1</sup>, Walt A. deHeer<sup>2</sup>, Lei Ma<sup>1,\*</sup>

<sup>1</sup>Tianjin International Center for Nanoparticles and Nanosystems, Tianjin University, 92 Weijin Road, Nankai

District, Tianjin 300072, China

<sup>2</sup>School of Physics, Georgia Institute of Technology, 837 North Ave, NW, Atlanta, Georgia, GA30332

Author to whom correspondence should be addressed: [lei.ma@tju.edu.cn](mailto:lei.ma@tju.edu.cn)

# These two authors contribute equally

## ABSTRACT

A cryogenic beam apparatus for studying neutral clusters has been built and tested. The lowest beam temperature reaches less than 9 K at a repetition rate of 20 Hz. Mechanical decoupling from the refrigerator avoids misalignment during temperature ramping. Adopting a permanent magnet based magnetic deflector eliminates the hysteresis and electric noise of the traditional electromagnet and offers excellent reproducibility of the applied magnetic field. The mass spectrometer can operate in either Mass Spectroscopy Time-Of-Flight (MSTOF) mode or Position-Sensitive Time-Of-Flight (PSTOF) mode with spatial resolution better than 7  $\mu\text{m}$ . Its performance is demonstrated with niobium and cobalt clusters.

## I. INTRODUCTION

Clusters are particles formed by two to several thousands of atoms or molecules. They are known for their strong size, shape, composition, and charge dependent properties, which are typically intermediate between those of isolated atoms or molecules and the bulk or solid-state materials.<sup>1</sup> Cluster physics is motivated by tracing the evolution of properties from the atom to the bulk<sup>2,3</sup> as well as identifying clusters of specific size that have unique properties. To explore these properties, several experimental techniques have been developed and intensively applied in the past four decades. Cluster science follows two major routes: studies of clusters deposited on a substrate<sup>4,5</sup> and free in the gas phase.<sup>6</sup> The latter avoids perturbations due to substrate interactions to allow the exploration of cluster's

intrinsic properties, which can be directly compared with theoretical predictions.<sup>7</sup> This approach includes photoelectron spectroscopy of size selected anionic clusters,<sup>8-10</sup> electron diffraction,<sup>11, 12</sup> X-ray magnetic circular dichroism,<sup>13,14</sup> optical spectroscopy,<sup>15</sup> cluster mobility<sup>16</sup> and photofragmentation.<sup>17</sup> As some of the earliest developed studies, magnetic and electric deflection<sup>18-21</sup> experiments were among the first to directly reveal the collective response of all the electrons in clusters to an external field, shedding light on understanding electronic correlations in small systems.<sup>22</sup>

Advances in the study of free clusters closely follow the development of new molecular and atomic beam methods. Notably, from the venerable experiments that realized the very first magnetic dipole moment measurements,<sup>23</sup> the famous Stern-Gerlach discovery of spin quantization<sup>24</sup> and the accurate measurement of velocity distributions of molecules in the gas phase.<sup>25</sup> Followed by the nuclear magnetic moment measurement by Rabi<sup>26</sup> and further improvements by Ramsey.<sup>27</sup> All relied on the invention and development of new molecular beam methods and apparatus.

The first magnetic deflection experiment in clusters was conducted in 1978<sup>28</sup> and was followed up by measuring static electric polarizabilities of sodium clusters.<sup>29</sup> Those experiments were performed in the machine built at the University of California, Berkeley, which embodied the first generation of electric and magnetic deflection mass spectrometers (1<sup>st</sup> EMDMS). Abundance spectra of sodium clusters measured in that machine unveiled their electronic shell structure,<sup>30</sup> which completed the remarkable trend of nature observed in atoms<sup>31</sup> and nuclei.<sup>32</sup> However, the apparatus was limited by the cluster types that can be generated in its source. Accordingly, a 2<sup>nd</sup> EMDMS was constructed with an improved laser vaporization source at Ecole Polytechnique Federale de Lausanne which could produce intense, stable and cold cluster beams with a temperature range from 100 K to 1000 K.<sup>33</sup> The design included a Time-Of-Flight mass spectrometer (TOFMS) with two modes, position-sensitive for cluster beam deflection measurements and high-mass-resolution mode with a resolution of about 1000.<sup>34</sup> The very first systematic study of size dependent magnetic property evolution of single-element ferromagnetic materials at the nanoscale was completed in that machine.<sup>19, 35</sup>

A third generation apparatus was built at the Georgia Institute of Technology, which was further equipped with a largely improved close-cycle cryogenic source with a precooled reservoir coupled with two pulse valves. It cools the generated clusters down to 20 K, which revealed electric dipole moments in neutral niobium clusters at low temperature<sup>36</sup> and the first example of multiferroic behavior in metal clusters.<sup>37</sup>

Similar facilities have been developed by several groups in the past few decades, such as the Dugourd 's,<sup>38</sup> Kresin's,<sup>20</sup> Bloomfield's,<sup>39</sup> Knickelbein's,<sup>40, 41</sup> Lievens and Ewald's,<sup>42</sup> and Schäfer's<sup>43, 44</sup> groups. Their working principle is roughly the same, but each one has its own specific features. It is worth to be noted that Kresin et. al have pioneered the study of the properties of extremely cold clusters embedded in helium droplets in a related apparatus.<sup>45</sup>

## II. EXPERIMENTAL SETUP

An overview of the setup is shown in Fig. 1. It consists of a newly designed pulsed laser vaporization source, an electron diffraction chamber, an interaction chamber, which includes an electrical deflection unit, a magnetic deflection unit and a standing wave grating<sup>46, 47</sup>, terminating in a TOFMS as detector.<sup>48, 49</sup>

The source is shown here having high cooling efficiency of clusters, and it is simpler compared to the one in the 3<sup>rd</sup> EMDMS with higher reliability. Briefly, inside the source, a short laser pulse is tightly focused onto the sample rod and creates a metal vapor cloud, then the vapor is cooled by a pulse of buffer gas (usually helium) where the vapor condenses to form clusters. After attaining thermal equilibrium with the buffer gas in the source, clusters exit through a nozzle. The clusters are carried in the buffer gas and pass through two sequentially aligned collimators. The cluster beam then interacts with an inhomogeneous field (electric or magnetic) or the photons of the optical standing wave grating in the interaction zone. After reaching the ionization zone of the TOFMS, the clusters are photoionized by a 157 nm laser. Finally, the cluster cations are subjected to the electric fields in the ionization zone causing them to fly through a drift tube to the detector. Their time of flight are measured from which their masses and deflections are determined and recorded. In the following paragraphs, we will describe (A) vacuum system, (B) cluster source, (C) velocity measurement unit, (D) deflection unit, (E) position sensitive time-of-flight mass spectrometer, (F) timing and data acquisition.

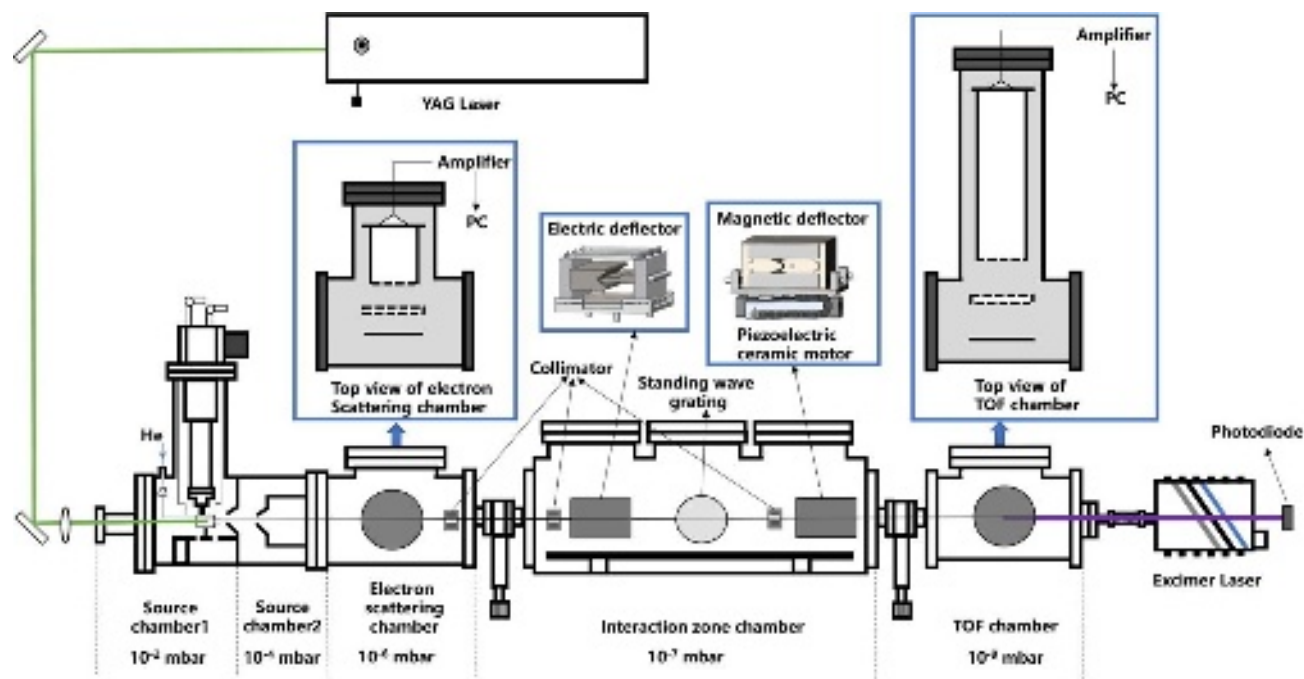


**FIG. 1.** Schematic overview of the cryogenic neutral cluster beam apparatus. It has electric and magnetic deflectors and a position sensitive mass spectrometer. The cluster source chamber and electron scattering chamber are connected via two skimmers. The electron scattering, interaction zone and Time-Of-Flight (TOF) mass spectrometer chambers are all connected by gate valves. The working pressures are noted. The distance between the nozzle and the first skimmer should be short enough to avoid excessive collisions in the source chamber, meantime, the diameter of the skimmer should be small enough to guarantee a good collimation of beam and differential pumping.

### A. Vacuum system

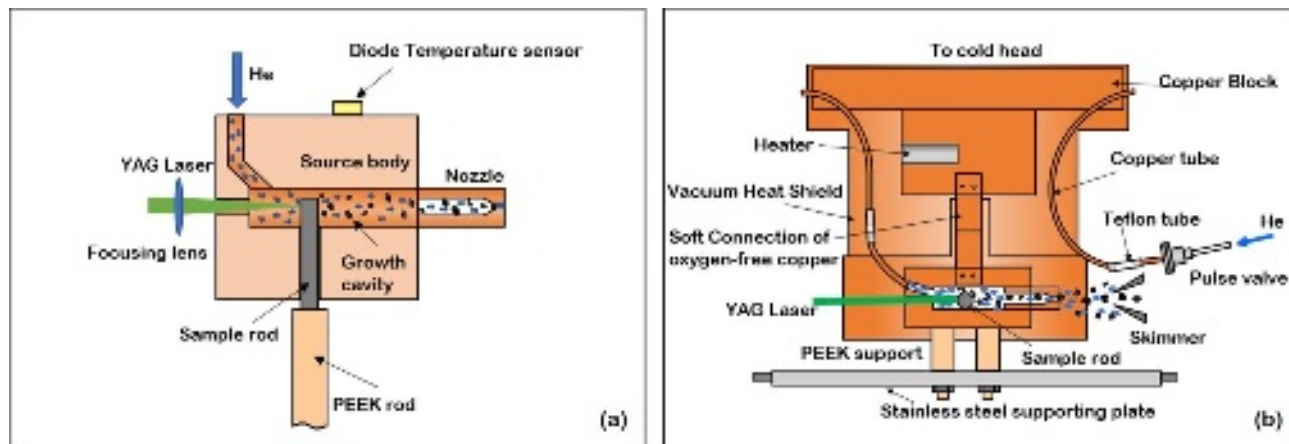
An ultrahigh vacuum is a prerequisite for free cluster measurements to ensure that the mean free path (MFP) is several orders higher than the dimension of the apparatus to minimize beam scattering. A large amount of helium injection is necessary to optimally operate the source, which requires a well-designed differential pumping system. Details and parameters of the vacuum system are presented in Fig. 1 and Table I.

Table I. Pressures of each chamber of the apparatus and the type of the vacuum pumps used in the system.

Chambers	Pumping	Working pressure	Background vacuum
Source chamber1	1 mechanic pump ( $10^{-3}$ mbar) serves as backing pump with 1 magnetic levitation turbo pump	$10^{-2}$ mbar	$10^{-7}$ mbar
Source chamber2	1 mechanic pump ( $10^{-3}$ mbar) serves as backing pump with 1 magnetic levitation turbo pump	$10^{-4}$ mbar	$10^{-7}$ mbar

<b>Electron scattering chamber</b>	Backing pumping ( $10^{-3}$ mbar) through foreline pumps with 1 magnetic levitation turbo pump	$10^{-6}$ mbar	$10^{-9}$ mbar
<b>Interaction zone chamber</b>	Backing pumping ( $10^{-3}$ mbar) through foreline pumps with 1 magnetic levitation turbo pump	$10^{-7}$ mbar	$10^{-9}$ mbar
<b>TOF chamber</b>	Backing pumping ( $10^{-3}$ mbar) through foreline pumps with 2 magnetic levitation turbo pumps	$10^{-9}$ mbar	$10^{-9}$ mbar

## B. Cluster source design



**FIG. 2.** Details of the cryogenic laser vaporization source. (a) Top view cross section. (b) Side view. (The Cold Head is a Sumitomo Dual Stage 1.5 W@4.2 K).

The dimensions of the newly designed cluster source are  $12.5 \text{ mm} \times 28 \text{ mm} \times 30 \text{ mm}$ , which is made of high-purity oxygen-free copper. As shown in Fig. 2 (a), it has a cylindrical cavity with a diameter of 5 mm and a length of 25 mm. The sample is inserted from a 1.5 mm diameter side hole into the cavity. Passing through a 1.5 mm diameter back-hole, 532 nm ablating YAG laser pulses are focused onto the sample surface. Right before each laser pulse, helium carrier gas is injected into the cavity through a channel with a diameter of 1.5 mm and a  $45^\circ$  angle with respect to the cavity axis.

The source is thermally coupled to a cold head of the cryogenic system through a bunched copper foil soft connection as shown in the supplementary material (Fig. S1), which overcomes the limitation due to the hard connection of the previous design and improves the flexibility of the source. In addition, the source stands on a stainless steel plate, which is welded to the inner wall of the chamber, with two PEEK (Polyether-Ether-Ketone) rods as thermal insulators, and anchored in a fixed position. This greatly improves the alignment of the beam and effectively eliminates disturbances to the cluster beam due to vibration of the cold head. The soft copper thermal connection ensures that the source remains well aligned during cooling or warming.

Well controlled temperatures are essential for free metal cluster physics experiments. Therefore, as in previous generations, the clusters are produced in a reservoir of volume  $V$  where the clusters dwell for sufficient amount of time to ensure thermalization with the precooled buffer gas at pressure  $p$ . Cooling in the expansion, as the beam exits through the nozzle, is determined by the terminal Mach number ( $M_T$ ), which depends on the product  $p \cdot D$ .<sup>50</sup> Hence, the diameter of the nozzle  $D$  is chosen so that this factor is small, obtaining a quasi-effusive beam. An essential design feature of the 3<sup>rd</sup> generation of sources is that the ratio of the number of collisions of the clusters with the buffer gas in the reservoir to the number of collision of clusters in the beam is on the order of  $V/D^3 \approx 1000$ . Experimentally, cluster equilibration with the source is checked by observing the dependency of a measured physical property with the cluster source temperature but not on the buffer gas pressure or the beam velocity. In short, the cluster source design specifically aims to equilibrate the clusters inside the source and to insure that the molecular beam expansion does not significantly affect the temperatures.

To accomplish these conditions, the previous generation cryogenic source used two pulse valves. There, the buffer gas (helium) was precooled to approximately 15 K in a reservoir that was filled with the first pulsed valve. This configuration successfully produced 20 K clusters. However, the directly applied custom-built cryogenic pulsed valve was prone to failure. In the new design, presented here, the reservoir and the first pulsed valve is replaced by a 30 cm long thin copper tube welded on the 40 K thermal shielding to serve the function of precooling (Fig. 2 (b)). Only one pulse valve is needed and directly mounted on the source chamber, operating at room temperature. For further thermal insulation, the copper tube is divided into three sections that are inter-connected by two Teflon tubes. The first Teflon tube follows the copper tube that is welded on the vacuum heat shield and the second precedes the copper tube that is attached to the source body, as shown in the supplementary material (Fig. S2).

The simplified design greatly improves the reliability, and reaches lower temperatures compared with the previous design as described below. As is shown in Fig. 2 (b), a 50 W heater is installed on the copper block, which together with the cold head and PID controller realizes accurate temperature control of the cluster source ranging from 6.7 K to 300 K with a resolution of 1 K. Photos of the cluster source is shown in the supplementary material (Fig. S3). More general discussions on the equilibrium between translational, vibrational, and rotational degrees of freedoms in molecular beam as well as the

differences between the beam ensemble and internal temperature of clusters can be found in Refs<sup>51-53</sup>.

### C. Velocity measurement unit

As the discussion above, in order for the temperature of clusters to be well-controlled requires that the beam is quasi effusive (see also Supplementary Material). Deflections are inversely proportional to the square of the cluster velocity. Therefore, accurate velocity measurements are crucial. The most common method is adopted that measures the velocity by chopping the beam into short pulses.<sup>54</sup> The flight-time of clusters from the chopper to the detector is defined by the drop in intensity when the blade interrupts the beam, and the beam velocity is calculated with the known flight length accordingly. Details of the velocity measurement method and mathematic derivations can be found in the supplementary material (Fig. S4-S5).

A supersonic expansion is realized when the gas pressure difference before and after expansion is large with the correct ratio between the relative aperture of skimmer and the mean free path of the buffer gas.<sup>55</sup> For lower pressure differences the beam is effusive, which in our case requires that the pressure behind the pulsed valve is less than 20 psi and the opening time of valve is adjusted to that the beam conditions are far below the threshold required for a supersonic expansion. The most probable speeds of background He gas are  $\sqrt{\frac{5K_B T}{m_{\text{He}}}}$  and  $\sqrt{\frac{3K_B T}{m_{\text{He}}}}$  for supersonic beam and effusive beam, respectively.<sup>56</sup> In contrast, in our case, it is close to  $\sqrt{\frac{2K_B T}{m_{\text{He}}}}$  when  $T \geq 15$  K and approach  $\sqrt{\frac{3K_B T}{m_{\text{He}}}}$  when  $T \leq 13$  K. For  $13 \text{ K} < T < 15 \text{ K}$ , the speeds are in between the two limits, suggesting a large velocity slip when temperature is higher than 15 K as shown in the supplementary material (Fig. S6). This indicates that the internal temperature of the clusters is not significantly affected by the expansion and remain close to the equilibrium temperature in the source.<sup>57</sup> Note that the dwell time in the source is sufficient to cool the clusters to the inert gas temperature as has been demonstrated in earlier generations of the source.<sup>19,36</sup> Additionally, the internal (i.e. vibrational and electronic) temperatures of the clusters are the most relevant criteria that address solid state properties of clusters. These 3N-6 internal degrees of freedom of a  $X_N$  cluster are difficult to cool and requires a large dwelling time in the source so that the number of collisions with the He carrier gas must be at least an order of magnitude larger than N. In contrast, fewer collisions are required to accelerate the cluster to the He beam speed. A large velocity slip indicates that the clusters have not had enough collisions with He to attain the carrier velocity, which means that the internal temperatures are expected to be close to that of the source.

This can be experimentally tested by measuring a temperature sensitive property at various carrier gas pressures to establish the quasi-effusive threshold for that property, as shown in the supplementary material (Fig. S7-S9). We have found that for this source a backing pressure of 20 psi is well lower than the threshold in the experiments discussed below.

#### D. Deflection unit

The cluster beam is collimated by a slit with width of 0.2, 0.4 or 0.8 mm upon the needs of measurements before entering the deflection unit, where the clusters are deflected by interacting with an inhomogeneous electric or magnetic field. Details of the interaction zone is shown in the supplementary material (Fig. S10).

The challenge of designing such a field is to generate an area with constant gradient large enough to accommodate the cross section of the beam. The two-wire field geometry is one solution which was first introduced by Rabi in 1934,<sup>58</sup> whose magnetic field gradient is uniform along the beam height direction, but varies greatly along the beam width. Therefore, D. McColm et al. designed a quadrupole-like magnet based on the two-wire field, the magnet of this structure can generate magnetic field with a uniform gradient over the cross-section of the collimated beam.<sup>59</sup> The two-wire field geometry and quadrupole-like geometry are the two most commonly used in molecular beam deflection experiments. Here, we choose the latter as shown in detail in the supplementary material (Fig. S11).

The inhomogeneous electrical field is generated by Rabi-type poles with a length of 200 mm and a minimum gap of 2.4 mm. The electric field and gradient are 80 kV/cm and 218 kV/cm<sup>2</sup> in the deflection area with a voltage of 20 kV across the poles. They are made of well-polished SS316 steel. Their front view is shown in the supplementary material (Fig. S12).

A newly designed permanent magnet deflector<sup>60-62</sup> is used instead of the conventional electromagnet to perform the magnetic deflection of beams.<sup>63-66</sup> The poles and yoke plates are made of Permendur and the magnetic field is produced by two cuboid magnets made from nickel-plated N52 neodymium, as shown in Fig.3 (a). It has the advantages of lower cost, simpler structure, zero electric noise, extremely consistent magnetic field distribution and zero hysteresis. In order to design and optimize our magnetic deflector, the magnetic field distribution was simulated through a Finite element method based program PANDIRA.<sup>67</sup> Table II lists the parameters that describe the optimal geometry of the permanent magnet deflector. The simulated results are plotted in Fig. 3 (b) and (c). A field

magnitude of  $1.02\text{ T}$  and gradient of  $420\pm 10\text{ T/m}$  are achieved with inhomogeneity of the gradient on the order of  $\pm 8\%$  for the beam area of  $2.8\times 0.3\text{ mm}^2$ .

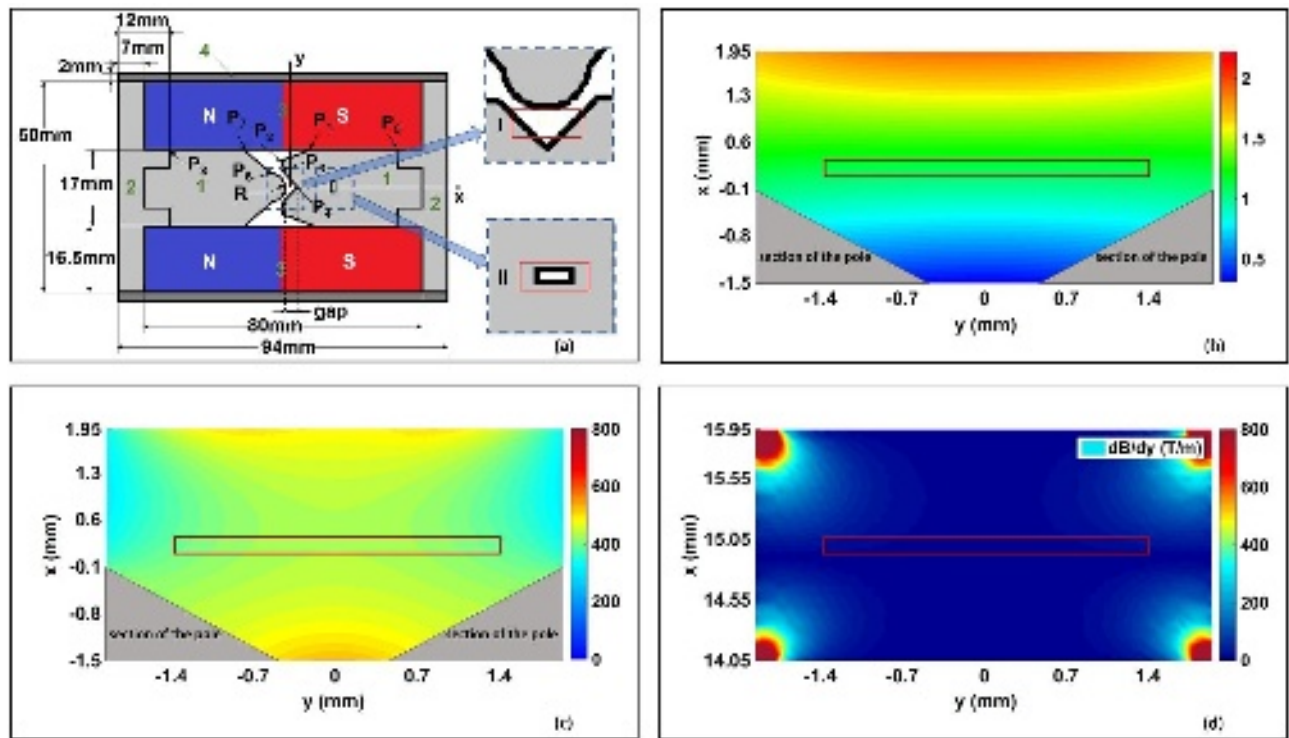


**FIG. 3.** (a) Front view of the magnetic deflector. 1. Pole shoes with the length of 200 mm; 2. Yoke; 3. Permanent magnets; 4. Holding plates made of stainless steel; 5. Rectangular hole for the passage of the undeflected beam. Close-up views of the central pole gap and rectangular hole are shown in the top right and bottom right of the figure, respectively, and the magnetic field and gradient inside the red boxes I and II are shown in (b), (c) and (d) accordingly. The small rectangle in the gap between the poles indicates the cross-section of the collimated cluster beam. (b) and (c) are simulated magnetic field and y-component of gradient in the gap; y is the horizontal direction and perpendicular to the beam velocity. (d) is the calculated magnetic field gradient in the  $2\times 4\text{ mm}^2$  rectangular hole.

Table II. Parameters of each pole (expressed in coordinates or length, unit: mm) used in the PANDIRA simulation.

The pole positions are measured with respect to the gap center as shown in Fig. 3 (a).

Position	Coordinate (mm)	Position	Coordinate (mm)
Gap	4	P <sub>4</sub>	(0, 2)
R	4	P <sub>5</sub>	(35, 8.5)
P <sub>1</sub>	(5, 8.5)	P <sub>6</sub>	(-4, 6)
P <sub>2</sub>	(-2.38, 6.96)	P <sub>7</sub>	(-16, 8.5)
P <sub>3</sub>	(-2.38, 4.96)	P <sub>8</sub>	(-35, 8.5)

A  $2\times 4\text{ mm}^2$  rectangular hole (Fig.3(a)) where the field gradient is close to zero, and cluster deflections are negligible. Hence, so called off-peak (field free) measurements can be obtained as

shown Fig.3(d). A piezoelectric ceramic motor (MICRONIX, PPS-60-10009) was installed to precisely switch the position of magnetic deflector from the deflection mode to the field free mode.

#### **E. Position sensitive TOF Mass Spectrometer**

After being deflected, clusters reach the detector chamber and are ionized by an F<sub>2</sub> excimer laser (157 nm, 2 mJ/pulse, 8 ns duration and 20 Hz). The ionized clusters are then accelerated in the electric field between repeller / extractor grid (R/E) and fly toward a microchannel plate (MCP) which is located at the end of the drift tube (more details are shown in Fig. S13). Ions impinging on the MCP generate electric pulses that are subsequently amplified by a fast broadband amplifier ORTEC, 9326 and then collected using a high-speed data acquisition card (spectrum, M4i.2211) in a computer.

The spectrometer can be operated in the mass spectroscopy mode or position-sensitive mode depending on the voltage settings of the electrodes as shown in the supplementary material (Fig. S14). There are two ways to run the system, one with delay-extraction, in order to effectively compensate the time error caused by the so called turn-over effect,<sup>68</sup> and another is the ionizing-accelerating mode which will keep the voltage constant so that the cluster will be accelerated instantly after it is ionized. Since this is within the laser pulse, the time resolution is limited by the width of laser pulse. However, for most systems of interest, this is not a significant problem so that this mode of operation is normally preferred since it makes the operation much simpler and the signals less noisy.

#### **F. Timing and data acquisition**

The system nominally runs at 20 Hz, i.e. 50 ms per cycle. Two multichannel delay pulse generators (SRS, DG535 and SRS, DG645) are used to set the timing sequence of the experiments, which is indicated in Fig. 4. After about 9 ms (when T = 20 K), the clusters arrive at the ionization region of the PSTOF spectrometer, at which time the excimer laser is triggered to fire and ionize them. Depending on the operation mode, the data acquisition card is triggered either by the photodetector or by the same trigger signal for the high voltage switch of the repeller. The timing sequence is controlled by a Labview program.

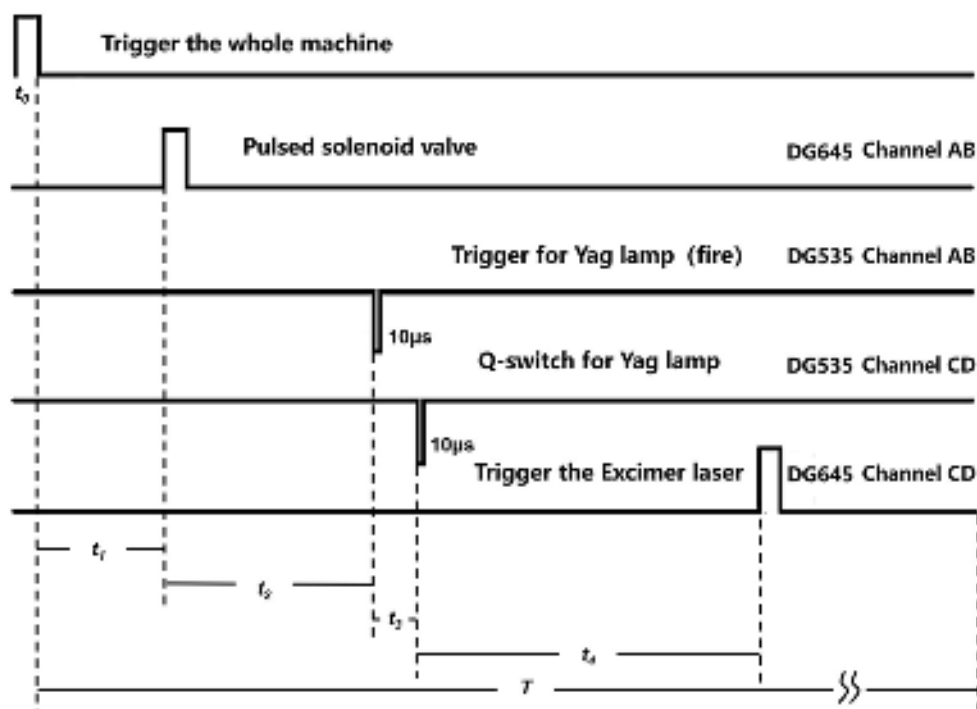


**FIG. 4.** Timing sequence of the experiment. The internal trigger mode of DG535 is used as the trigger of the experiment to set the 20 Hz repetition rate and the initiation  $t_0$ . Following the trigger, after  $t_1$  time interval, the pulsed solenoid valve is turned on first to let the gas into the source in advance. After time interval  $t_2$ , the YAG laser is engaged with Q-delay of  $t_3$  to fire and ablate the sample rod, leading to a plasma and rapidly cooled in the helium atmosphere to form the targeting clusters. The  $t_3$  is delay between the lamp firing and Q-switch of the YAG laser depends on the required laser energy for target ablation. The excimer laser is triggered to ionize clusters with a time delay  $t_4$  from the YAG laser firing.  $T$  is one experimental period, equal to 50 ms.

### III. RESULTS AND DISCUSSION

In this section, we demonstrate the performance and capability of the machine in the following aspects: mass resolution in the MSTOF mode, the reachable lowest temperature, and the PSTOF spectrum of Nb clusters.

#### A. Low temperature MSTOF mode

The temperature of the source body is measured with a silicon diode (East Changing, DT64-B0-4L). The cryocooler has 45 W of cooling power at 40 K, and 1.5 W at 4.2 K. The source body can be cooled down to  $6.9 \pm 1$  K without gas loading and the lowest reachable temperature of the source body with gas loading is  $8.7 \pm 1$  K, so far. Fig. 5 displays a mass spectrum of niobium clusters acquired in a mass-spectroscopy mode at  $8.7 \pm 1$  K (source body temperature). A close-up peak of  $\text{Nb}_{21}$  is shown in

the inset which indicates a mass resolution of  $\frac{m}{\Delta m}=1528$ . As discussed above, the main factor limiting the mass resolution is the 8 ns long ionization laser pulse. Even though, it is sufficient to get atomic resolution in clusters that contain several hundred atoms.

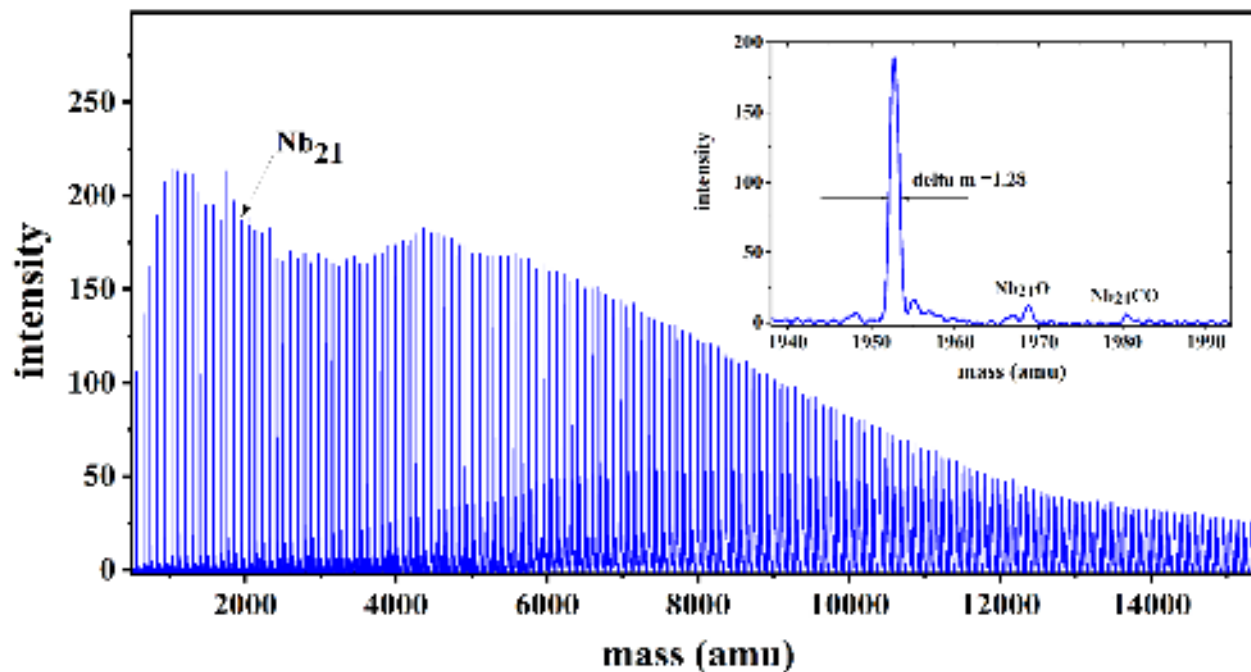


**FIG. 5.** TOFMS of  $Nb_N$  clusters obtained at a source temperature  $8.7 \pm 1$  K and a close-up view of  $Nb_{21}$  in the inset. The weaker peaks are  $Nb_NO$  and  $Nb_NCO$ , which may come from the leftover oxygen and surface coated carbon in the source cavity during vaporization.

The beam velocity measurements have been conducted which indicate a most probable velocity of about  $230 \pm 8.5$  m/s as shown in the supplementary material (Fig. S5). Further analysis indicate the cluster temperature is close to the source temperature of  $8.7 \pm 1$  K, which is consistent with the quasi-effusive cluster beam described above as shown in the supplementary material (Fig. S6).

### B. Low temperature PSTOF mode

The position sensitivity of PSTOF is calibrated using an accurately position controlled mobile slit with width of 0.4 mm that is placed in front of the ionization laser as shown in the supplementary material (Fig. S15), demonstrating that the position resolution is better than  $7 \mu\text{m}$ .

Two representative electric deflection beam profiles of position-sensitive mass spectra of niobium clusters are shown in Fig. 6. The neutral cluster beam is collimated with a 0.4 mm slit before entering into the inhomogeneous field region and then deflected to measure their polarizabilities. The on-peak

of  $\text{Nb}_{15}$  exhibits a uniform deflection toward high field, however,  $\text{Nb}_{14}$  is broadened with reduced intensity compared with the off-peak. This agrees with the previous observations in ref [36] but with a larger depletion ratio, which is consistent with the lower temperature of these clusters compared with Ref. 36.

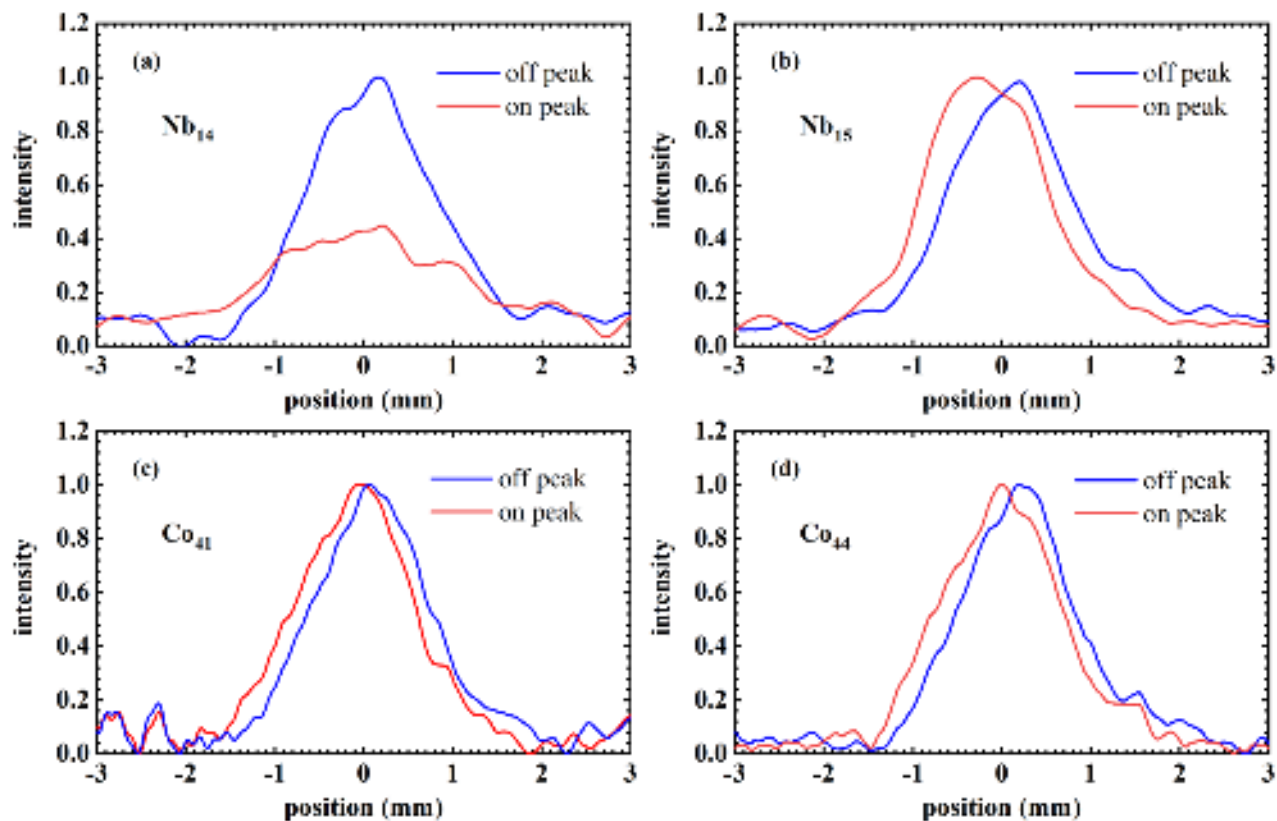


**FIG. 6.** Several test deflection results: (a) and (b) Electric deflection profiles of two representative niobium clusters recorded with PSTOF at  $T_{\text{source}}=8.7\pm 1$  K with (red) and without (blue) applied deflection voltage of 18 kV. (c) and (d) are magnetic deflection profiles of  $\text{Co}_{41}$  and  $\text{Co}_{44}$  at  $T_{\text{beam}}=50.5\pm 1$  K with the newly built permanent magnet deflector.

The agreement with previously published results using a substantially different source, ensure the reliability of the current apparatus and reconfirm the results obtained 20 years ago. Furthermore, it demonstrates the effect of lower temperatures that were previously not obtainable. Moreover, the lower temperature produces slower beam speed, and correspondingly larger deflections for the dipole moments established at the higher temperatures.

#### IV. CONCLUSION

A new neutral cluster beam machine has been built to study electric and magnetic properties of neutral clusters. The mass resolution of spectrometer is over 1500, so that clusters with up to 1000 atoms with a single element can be identified with atomic resolution. This range can be further increased by applying pulsed extraction in the MSTOF. The flexible design makes it versatile to do

different experiments in the future, such as, scattering of helium atoms, low energy electron scattering, and others. The crucial improvement with respect to previous designs is that the cryogenic pulse laser vaporization source can cool the clusters down to less than 9 K at a pulse frequency of 20 Hz. The lower temperature has the immediate advantage of slower velocities and concomitant higher sensitivity in deflection experiments. Most importantly, the lower temperatures allow the exploration of novel condensed matter phenomena in well-defined finite systems, as for example in Ref. 36.

### Supporting information

Supplementary information including photographs and figures of cluster source, principle and results of velocity measurement, figures of interaction zone chamber and deflection unit, principle and calibration of Position Sensitive TOF Mass Spectrometer.

### ACKNOWLEDGMENTS

This work was supported by the National Natural Science Foundation of China under Grant No. 11774255 and the National Key R&D Program of China No. 2020YFC2004602.

### Declarations

The authors have no conflicts to disclose.

### REFERENCE

- <sup>1</sup> W. A. de Heer, Rev. Mod. Phys. **65**, 611 (1993).
- <sup>2</sup> A. J. Cox, J. G. Louderback, S. E. Apsel and L. A. Bloomfield, Phys. Rev. B **49**, 12295 (1994).
- <sup>3</sup> R. Kusche, T. Hippler, M. Schmidt, B. von Issendorff and H. Haberland, Eur. Phys. J. D. **9**, 1 (1999).
- <sup>4</sup> J. Gittleman, B. Abeles and S. Bozowski, Phys. Rev. B **9**, 3891 (1974).
- <sup>5</sup> C. Xirouchaki and R. Palmer, Phil. Trans. R. Soc. Lond. A **362**, 117 (2004).
- <sup>6</sup> S. Y. van de Meerakker, H. L. Bethlem, N. Vanhaecke and G. Meijer, Chem. Rev. **112**, 4828 (2012).
- <sup>7</sup> J. Li, X. Li, H. J. Zhai and L. S. Wang, Science **299**, 864 (2003).
- <sup>8</sup> A. Stolow, A. E. Bragg and D. M. Neumark, Chem. Rev. **104**, 1719 (2004).
- <sup>9</sup> L. Lehr, M. Zanni, C. Frischkorn, R. Weinkauf and D. Neumark, Science **284**, 635 (1999).

- <sup>10</sup> I. León, Z. Yang, H. T. Liu and L. S. Wang, *Rev. Sci. Instrum.* **85**, 083106 (2014).
- <sup>11</sup> X. Xing, B. Yoon, U. Landman and J. H. Parks, *Phys. Rev. B* **74**, 165423 (2006).
- <sup>12</sup> A. Lechtken, C. Neiss, M. M. Kappes and D. Schooss, *Phys. Chem. Chem. Phys.* **11**, 4344 (2009).
- <sup>13</sup> J. Lau, A. Föhlisch, R. Nietubyc, M. Reif and W. Wurth, *Phys. Rev. Lett.* **89**, 057201 (2002).
- <sup>14</sup> M. Niemeyer, K. Hirsch, V. Zamudio-Bayer, A. Langenberg, M. Vogel, M. Kossick, C. Ebrecht, K. Egashira, A. Terasaki and T. Möller, *Phys. Rev. Lett.* **108**, 057201 (2012).
- <sup>15</sup> W. A. de Heer, K. Selby, V. Kresin, J. Masui, M. Vollmer, A. Chatelain and W. Knight, *Phys. Rev. Lett.* **59**, 1805 (1987).
- <sup>16</sup> D. E. Clemmer and M. F. Jarrold, *J. Mass Spectrosc.* **32**, 577 (1997).
- <sup>17</sup> J. Tiggesbäumker, L. Köller, H. Lutz and K. H. Meiwes Broer, *Chem. Phys. Lett.* **190**, 42 (1992).
- <sup>18</sup> R. Schäfer, S. Schlecht, J. Woenckhaus and J. Becker, *Phys. Rev. Lett.* **76**, 471 (1996).
- <sup>19</sup> I. M. Billas, A. Chatelain and W. A. de Heer, *Science* **265**, 1682 (1994).
- <sup>20</sup> G. Tikhonov, V. Kasperovich, K. Wong and V. Kresin, *Phys. Rev. A* **64**, 063202 (2001).
- <sup>21</sup> R. Antoine, P. Dugourd, D. Rayane, E. Benichou, M. Broyer, F. Chandezon and C. Guet, *J. Chem. Phys.* **110**, 9771 (1999).
- <sup>22</sup> K. D. Bonin and V. V. Kresin, *Electric-dipole polarizabilities of atoms, molecules, and clusters* (World Scientific, Singapore, 1997).
- <sup>23</sup> H. Kallmann and F. Reiche, *Z. Phys.* **6**, 352 (1921).
- <sup>24</sup> W. Gerlach and O. Stern, *Z. Phys.* **9**, 349 (1922).
- <sup>25</sup> I. Estermann, O. Simpson and O. Stern, *Phys. Rev.* **71**, 238 (1947).
- <sup>26</sup> I. I. Rabi, S. Millman, P. Kusch and J. R. Zacharias, *Phys. Rev.* **55**, 526 (1939).
- <sup>27</sup> N. F. Ramsey, *Phys. Rev.* **78**, 695 (1950).
- <sup>28</sup> W. Knight, R. Monot, E. Dietz and A. George, *Phys. Rev. Lett.* **40**, 1324 (1978).
- <sup>29</sup> W. Knight, K. Clemenger, W. A. de Heer and W. A. Saunders, *Phys. Rev. B* **31**, 2539 (1985).
- <sup>30</sup> W. Knight, K. Clemenger, W. A. de Heer, W. A. Saunders, M. Chou and M. L. Cohen, *Phys. Rev. Lett.* **52**, 2141 (1984).
- <sup>31</sup> N. Bohr, *Philos. Mag.* **26**, 1 (1913).

- <sup>32</sup> M. G. Mayer, Phys. Rev. **75**, 1969 (1949).
- <sup>33</sup> W. A. de Heer and P. Milani, Z. Phys. D **20**, 437 (1991).
- <sup>34</sup> W. A. de Heer and P. Milani, Rev. Sci. Instrum. **62**, 670 (1991).
- <sup>35</sup> I. M. Billas, J. Becker, A. Châtelain and W. A. de Heer, Phys. Rev. Lett. **71**, 4067 (1993).
- <sup>36</sup> R. Moro, X. Xu, S. Yin and W. A. de Heer, Science **300**, 1265 (2003).
- <sup>37</sup> L. Ma, R. Moro, J. Bowlan, A. Kirilyuk and W. A. de Heer, Phys. Rev. Lett. **113**, 157203 (2014).
- <sup>38</sup> M. Abd El Rahim, R. Antoine, L. Arnaud, M. Barbaire, M. Broyer, C. Clavier, I. Compagnon, P. Dugourd, J. Maurelli and D. Rayane, Rev. Sci. Instrum. **75**, 5221 (2004).
- <sup>39</sup> D. Douglass, A. Cox, J. Bucher and L. Bloomfield, Phys. Rev. B **47**, 12874 (1993).
- <sup>40</sup> M. B. Knickelbein, J. Chem. Phys. **116**, 9703 (2002).
- <sup>41</sup> M. B. Knickelbein, J. Chem. Phys. **115**, 10450 (2001).
- <sup>42</sup> N. T. Tung, "Stability of bimetallic clusters and development of a magnetic deflection setup," Ph.D. dissertation (KU Leuven, 2014).
- <sup>43</sup> S. Schäfer, M. Mehring, R. Schäfer and P. Schwerdtfeger, Phys. Rev. A **76**, 052515 (2007).
- <sup>44</sup> U. Rohrmann, S. Schäfer and R. Schäfer, J. Phys. Chem. A **113**, 12115 (2009).
- <sup>45</sup> B. S. Kamerin, J. W. Niman and V. V. Kresin, J. Chem. Phys. **153**, 081101 (2020).
- <sup>46</sup> O. Nairz, B. Brezger, M. Arndt and A. Zeilinger, Phys. Rev. Lett. **87**, 160401 (2001).
- <sup>47</sup> S. Gerlich, L. Hackermüller, K. Hornberger, A. Stibor, H. Ulbricht, M. Gring, F. Goldfarb, T. Savas, M. Müri and M. Mayor, Nature Phys. **3**, 711 (2007).
- <sup>48</sup> W. Wiley and I. H. McLaren, Rev. Sci. Instrum. **26**, 1150 (1955).
- <sup>49</sup> J. Dawson and M. Guilhaus, Rapid Commun. Mass Spectrom. **3**, 155 (1989).
- <sup>50</sup> M. D. Morse, "Supersonic beam sources," in *Experimental methods in the physical sciences*, edited by F. B. Dunning and R. G. Hulet (Academic press, New York, 1996).
- <sup>51</sup> X. Xu, "The magnetism of free cobalt clusters measured in molecular beams," Ph.D. dissertation (Georgia Institute of Technology, 2007).
- <sup>52</sup> I. Billas, "Magnetism of iron, cobalt and nickel clusters studied in molecular beams," Ph.D. dissertation (Verlag nicht ermittelbar, 1995).
- <sup>53</sup> J. van der Tol and E. Janssens, Phys. Rev. A **102**, 022806 (2020).

- <sup>54</sup> G. Scoles, *Atomic and molecular beam methods* (Oxford university press, New York, 1988).
- <sup>55</sup> F. B. Dunning and R. G. Hulet, *Atomic, molecular, and optical physics: Atoms and molecules* (Academic Press, New York, 1996).
- <sup>56</sup> J. Anderson and J. Fenn, *Phys. Fluids* **8**, 780 (1965).
- <sup>57</sup> E. Kolodney and A. Amirav, *Chemical physics* **82**, 269 (1983).
- <sup>58</sup> I. I. Rabi, J. Kellogg and J. Zacharias, *Phys. Rev.* **46**, 157 (1934).
- <sup>59</sup> D. McColm, *Rev. Sci. Instrum.* **37**, 1115 (1966).
- <sup>60</sup> J. Liang, T. M. Fuchs, R. Schäfer and V. V. Kresin, *Rev. Sci. Instrum.* **91**, 053202 (2020).
- <sup>61</sup> K. P. Ziock and W. Little, *Rev. Sci. Instrum.* **58**, 557 (1987).
- <sup>62</sup> Y. Y. Fein, A. Shayeghi, L. Mairhofer, F. Kialka, P. Rieser, P. Geyer, S. Gerlich and M. Arndt, *Physical Review X* **10**, 011014 (2020).
- <sup>63</sup> D. Cox, D. Trevor, R. Whetten, E. Rohlfing and A. Kaldor, *Phys. Rev. B* **32**, 7290 (1985).
- <sup>64</sup> J. Bucher, D. Douglass, P. Xia, B. Haynes and L. Bloomfield, *Z. Phys. D* **19**, 251 (1991).
- <sup>65</sup> T. Hihara, S. Pokrant and J. Becker, *Chem. Phys. Lett.* **294**, 357 (1998).
- <sup>66</sup> M. B. Knickelbein, *Phys. Rev. Lett.* **86**, 5255 (2001).
- <sup>67</sup> K. Halbach, *Part. Accel.* **7**, 1 (1976).
- <sup>68</sup> R. M. Whittal and L. Li, *Anal. Chem.* **67**, 1950 (1995).

